introduces a hypothesis that the two strong absorptions at 2.74 THz and 2.84 THz, which are predicted to be an inter-molecular hydrogen bond network, would be derived from the common molecular structures of these compounds, and they form a hydrogen bond network with the neighboring molecule. Furthermore, the functional group which forms this hydrogen bond network would be located far from the aromatic hydroxyl group. This hypothesis suggests that a functional group such as [-NH_3^+], [-COO^-] would form the main hydrogen bond network in their crystalline structure. Further study is necessary to provide evidence for this hypothesis. The authors believe that the melting points of these compounds will provide an important hint to consider the hypothesis. For example, the melting points of *p*-tyrosine, *m*-tyrosine, and *o*-tyrosine, which have a hydroxyl group in their molecule structures, are reported to be 343 °C, 280-285 °C and 256 °C, respectively. *p*-Tyrosine and *m*-tyrosine, which are predicted to form a hydrogen bond network with the aromatic hydroxyl group, have strong absorptions. The intensity of absorption would be correlated not only with the strength of the inter-molecular hydrogen bond network but also with the melting points of these compounds. Moreover, *o*-tyrosine, which would form the hydrogen bond network without the aromatic hydroxyl group, has the lowest melting point. This fact suggests that a stronger inter-molecular hydrogen bond network formed by the aromatic hydroxyl group contributes the stable crystalline structure. On the other hand, the authors believe that phenylalanine (mp: 283 °C), which has a symmetric molecule structure, is more stable than *o*-tyrosine (mp: 256 °C). The authors presume that *p*-tyrosine forms a very stable crystalline structure based not only on the strong domination of the inter-molecule hydrogen bond derived from the aromatic hydroxyl group at 2.43 THz but also on the strong domination of the hydrogen bond that is detected at 2.14 THz. For example, the order of the melting points of the three compounds corresponds to that of the THz absorbance intensities derived from the strongest absorptions, which are assumed to form the inter-molecular hydrogen bond network with the adjacent molecules. This observation suggests that the intensities of terahertz absorptions may become one of the indicators of crystalline stability formed from a single molecule. Further study concerning the relationship between THz absorption and physical properties is necessary and requires the accumulation of data obtained from various compounds.

The absorption at about 2.4 THz was observed in all of the structural isomers of tyrosine that were used in this study. The terahertz electromagnetic region can detect not only intra-molecular vibrations but also inter-molecular vibrations such as hydrogen bonds. Therefore, distinguishing between intra- and inter-molecular vibrations using only terahertz absorptions would be quite difficult. The authors examined the prediction of intra-molecular vibrations in the terahertz region with the combination of a structural optimization simulation using the Gaussian function and mid-infrared absorptions. The distinguishability of absorptions between the intra- and inter-molecular vibrations was shown. This combination prediction procedure would provide useful information for assigning terahertz absorptions.

Table 1 Predicted frequency of intra-molecular vibration in terahertz electro-magnetic region
(Simulated by Gaussian 03 with B3LYP/6-31G(d))

Phenylalanine	*o*-Tyrosine	*m*-Tyrosine	*p*-Tyrosine
1.08 THz	1.03 THz	1.10THz	1.07 THz
2.43 THz	2.38 THz	2.30 THz	1.87 THz
2.98 THz	2.94 THz	2.98 THz	2.97 THz

Table 2 Frequencies of absorptions observed in the terahertz spectra of 4 kinds of compounds

Phenylalanine	0.94		1.56	1.82	2.03				2.84 (s)		3.26*
o-Tyrosine		1.13*	1.64		1.98		2.22	2.41*	2.74 (s)	3.02*	3.24* (s)
m-Tyrosine		1.13*	1.59	1.79 (s)			2.22	2.41*	2.65	2.83	3.02*	3.24* (s)
p-Tyrosine		1.12*				2.14 (s)		2.43 (vs)		2.85		3.23*

- The underlined frequencies represent commonly observed absorptions.
- The frequencies marked with a star (*) correspond to the simulated intra-molecular vibrations.

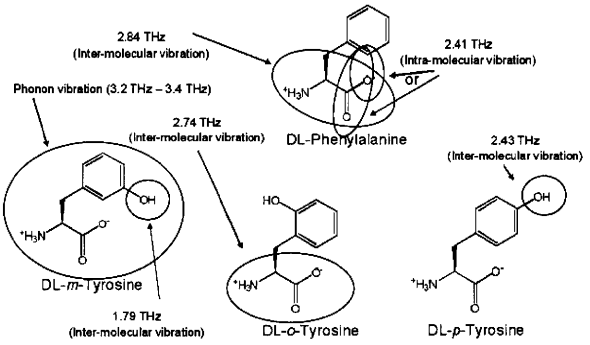

Fig. 1 Predicted intra- and inter-molecular vibrations based on the comparison of terahertz absorptions among four compounds and on Gaussian 03 simulation

ACKNOWLEDGEMENTS

This study was supported in part by a research grant from the Ministry of Health, Labour and Welfare of Japan (H20-iyaku-ippan-004).

978-1-4244-6656-6/10/$26.00 ©2010 IEEE

Coating evaluation of commercial tablets using Terahertz Pulsed Spectroscopy and Imaging

Tomoaki Sakamoto, Toru Kawanishi and Yukio Hiyama
National Institute of Health Sciences, 1-18-1, Kami-yoga, Setagaya-ku, Tokyo 158-8501, Japan

Alessia Portieri, Philip F. Taday and Donald D. Arnone
TeraView Limited, Platinum building, St. John's Innovation Park, Cambridge CB4 0WS, United Kingdom

Daisuke Sasakura, Tomoyuki Matsubara, Tsuyoshi Miura
Bruker Optics K.K., Takara Building 6F, 1-6-4, Taito, Taito-ku, Tokyo 110-0016, Japan

Abstract— In this study the authors have investigated coating thickness variations in film- and enteric-coated commercial tablets by means of Terahertz Pulsed Spectroscopy and Imaging (TPS/TPI). Unique THz images of density distribution in these commercial tablets were also obtained. Coating thickness, and its distribution, density of components by compression, and defects on the surface of these tablets, could be observed by TPS/TPI technique.

I. Introduction

Time-Domain THz Spectroscopy and Imaging (TDS / TDI) can be used to acquire structural and physical information such as an existence of layers and a change of density by delayed reflectance derived from a change of refractive index of THz pulse. The time-function obtained from TDS/TPI also provides information such as a thickness of coating layer. In this study, CPFX.HCl film-coated tablets and ASP enteric coated tablets, which are important and widely used, were selected. In both tablets, the coating has very important role to protect degradation of API by light and/or humidity for the former tablet and to prevent disintegration of tablet in a stomach for the latter tablet. The authors examined applicability of THz Pulsed Imaging technique to analyze the coating status and the density of components inside tablet and to evaluate its distinguishability among several kinds of commercial tablets which have same clinical application.

II. Experimental

A. Materials

Four kinds of CPFX.HCl tablets and three kinds of ASP tablets were purchased from commercial source. Polyethylene (< 80μm) that was used to prepare the sample pellets was purchased from Induchem AG (Volketswil, Switzerland).

B. Instruments and Measurement conditions

THz images of tablets were obtained using TPI imega 2000 system "Coating Scan" (TeraView Limited, Cambridge, UK). The rapid scan mode was used and images were constructed at 100μm of spatial resolution.

III. Results And Discussions

A. Ciprofloxacin hydrochloride Film-coated tablets

I) Plane THz images at 260μm depth: Figure 1 shows the THz images of distribution of relative refractive index changes in the plane of 260 μm depth from the surface of the tablets. In the images of the tablets A and D, the changes of refractive indices at the center of the tablets were larger than the edge of the tablets. And the tablet B showed comparatively large change of refractive indices through the wider area of tablet. In the image of the tablet C, the small areas which had comparatively small change of refractive indices were observed in the center of the tablet. Then, the area which had relatively higher refractive indices was observed at the edge of the tablet. These observations indicate that physical or mechanical status, such as uneven distribution of various particle sizes of granules or uneven penetration of compression force in a mortar derived from the manufacturing process will change a density of tablet components.

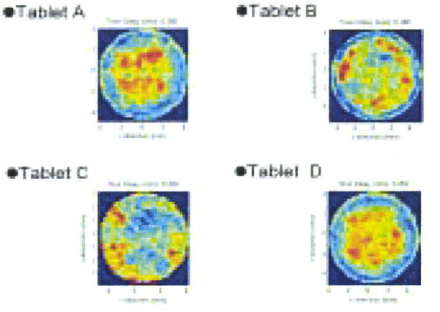

Fig.1 THz images of four kinds of the commercial tablets
(at the 260μm depth from the surface)

2) In depth images: The depth (B-Scan) THz images obtained from the commercial tablets A-D are shown in Fig. 2. The thickness of the coating layers in these tablets are approximately 100 μm. The left side and the right side of the bold line represent an air, and the inside of the tablet, respectively. The echoes which show several layers formed by compression are observed. The definite layers up to 1 mm-depth and up to 0.5 mm-depth were observed in the Tablet A and C, respectively. The fuzzy echoes were observed in the Tablet D. On the other hand, no definite but layer-like echoes were observed in the Tablet B. And those observations suggest that the force of compression was unevenly penetrated into the tablet.

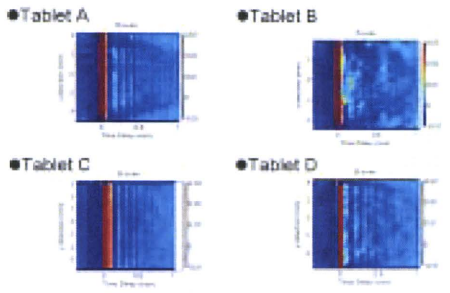

Fig.2 Depth (B-Scan) THz images of four kinds of the commercial tablets
(The right side from the bold lines represents inside tablets)

B. Aspirin Entero-coated tables

Figure 3 (A) shows the THz images concerning distribution of the coating thickness on the ASP tablet. The depth THz images which are shown in the right side of Fig 3 (A) represent the vertical planes against y-direction at the suitable x-points located in the broken circles which are seen in the images. The coating thicknesses in the circle in the above B-scan image distribute homogeneity, and the range of the coating thickness is from 95 μm to 100 μm. On the other hand, the circle in the below B-Scan image is shown the area which has comparatively high coating thickness, more than 110 μm. The visible ray image and the THz image on the tablet surface area obtained from the ASP Tablet are also shown in Fig.3 (B). The surface of the tablet is very smooth, and no protuberance on the surface at the high coating thickness area is observed. Moreover, the above B-scan image indicates an existence of hollow on the surface of the plain tablet (Fig.3 (A)). The below B-scan image shows the flat coating layer. These results suggest that the hollow on the surface of the plain tablet was buried by sprayed coating liquid and then additional sprayed coating liquid made flat coating layer and smooth surface on the tablet.

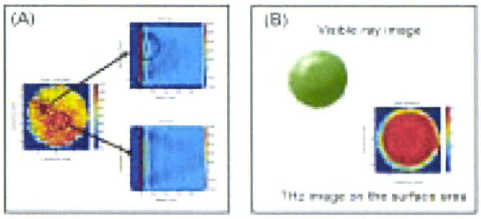

Fig. 3 THz images of ASP tablet A
(A: Left: distribution of coating thickness. Right: depth images. B: the visible ray image (Left) and the THz image on the tablet surface (Right))

IV. Conclusion

Coating thicknesses and their distribution, a density of components by compression, and hollows on a surface of tablet, which are based on detecting the delayed reflection of THz pulse can be observed by THz imaging technique. Detection of a coating status and a physical status change of tablet inside would contribute not only for identification of manufacturing quality but also for qualitative confirmation of commercial tablets including fake and/or defective products. THz pulsed spectroscopy and imaging technique will be useful as a non-destructive analytical tool for quality control of commercial tablets.

Acknowledgment

This study was supported in part by a research grant from the Ministry of Health, Labour and Welfare of Japan (H20-iyaku-ippan-004).

Malaysian Journal of Chemistry, 2009, Vol. 11, No. 1,088 - 093

Chiral Analysis of Re-crystallized Mixtures of D-, L-amino Acid Using Terahertz Spectroscopy

Tomoaki Sakamoto[1], Tadao Tanabe[2], Tetsuo Sasaki[3], Yutaka Oyama[2], Jun-ichi Nishizawa[3], Toru Kawanishi[1], Yukio Hiyama[1]

[1]Division of Drugs, National Institute of Health Sciences, Tokyo 158-8501, Japan
[2]Graduate School of Engineering, Tohoku University, Sendai 980-8579, Japan
[3]Center for Priority Area, Tokyo Metropolitan University, Tokyo 192-0397, Japan
Corresponding author email address: tsakamot@nihs.go.jp

Abstract: Distinguishability by terahertz absorption between D- and L-amino acids and a change in terahertz absorption based on the re-crystallization condition was examined. Terahertz spectra which were obtained from the re-crystallized each enantiomer or mixtures of D- and L-leucine or alanine were compared with those of the purchased reagents. The peak tops of the re-crystallized L- and D-leucine mixtures were shifted toward low frequency side and the half width of the peak at 3.7 THz became narrow to approximately half of that of the reagent. Difference of spectral features from 2.1 THz to 2.8 THz in the THz spectra between D- and L-alanines was observed. According to the result of peak separation against these spectra, distinction between the purchased D- and L-alanine was possible to compare the intensities of the sub-peaks. Moreover, changes of the integrated values of the peaks obtained from L- or D-form-rich mixture of leucine were observed. These results suggested that feasibility of chiral analysis of enantiomers using terahertz spectroscopy would be shown.

Keywords: Terahertz spectroscopy, polymorphs, enantiomers, crystals

Introduction

Terahertz (THz) electro-magnetic region (0.1 THz to 10 THz, 3.3 cm^{-1} to 333 cm^{-1}) detects a weak inter-molecular energy such as a hydrogen bond, and a crystal lattice vibration. In the pharmaceutical and the chemical industries, detection of polymorphs (1-8) and unique THz spectra obtained from active pharmaceutical ingredients (APIs), illegal drugs and explosives have been reported (1, 3, 6). The hydrogen bond and van der Waals force, which contribute to form the function-able structure of protein and amino acids, would be sensitively detected in THz region. Thus, absorption on THz electro-magnetic region would be expected to provide useful information for investigation of the function and the dynamics of these compounds. Amino acids which are components of protein are used as not only a supplement for keeping health but also a medication for certain diseases. Amino acids have hydrogen bond network in their crystals. Thus, an investigation concerning property of hydrogen bonds and intermolecular interactions would be useful to understand the functions of these compounds. Moreover, amino acids exist as L-form in nature, and their biological function is different by stereo- configuration. In study about an optical isomerism by THz spectroscopy, distinction between racemate and enantiomer by THz peaks has been reported (9, 10). However, distinguishability between both enantiomers has not been established yet. The authors examined the THz spectral change of the re-crystallized amino acids, leucine and alanine using THz electro-magnetic wave.

Materials and Methods

L-, D- and DL-leucine (racemate), and L-, D-, and DL-alanine (racemate) were purchased from Wako Pure Chemical Industries, Ltd. (Osaka, Japan). Polyethylene powder for making pellets was purchased from THz Laboratory Co., Ltd. (Akita, Japan).

Re-crystallization of these compounds was performed with water. Sample powder was dissolved in water at around 90 ºC and cooled down to room temperature. Then, this solution was put into a refrigerator at 4 ºC. Re-crystallized sample was filtered and washed with iced water, and dried in a desiccator under reduced pressure. The mixture of L- and D-amino acids which contains 25 % or 75 % of L-enantiomer was re-crystallized to make D- or L-form-rich mixed sample. The re-crystallized sample was diluted to concentration of 0.25 mol/l with polyethylene powder and then the mixture was compressed at 9.8 kN for 2 min to make pellets for transmittance measurements.

Measurements of THz spectra were performed by the Gallium-Phosphorus (GaP) THz signal generator system equipped with a pyroelectric DTGS detector. This THz generator system has been developed and constructed by Nishizawa et al (11-19). The optical system of this instrument is shown in Fig. 1. The spectra were measured from 1 THz (33 cm^{-1}) to 5 THz (167 cm^{-1}) at 15 GHz measurement steps. Measurements of optical rotations of the re-crystallized D-, L-amino acids and their mixtures were performed using DIP-360 polarimeter (JASCO, Tokyo, Japan).

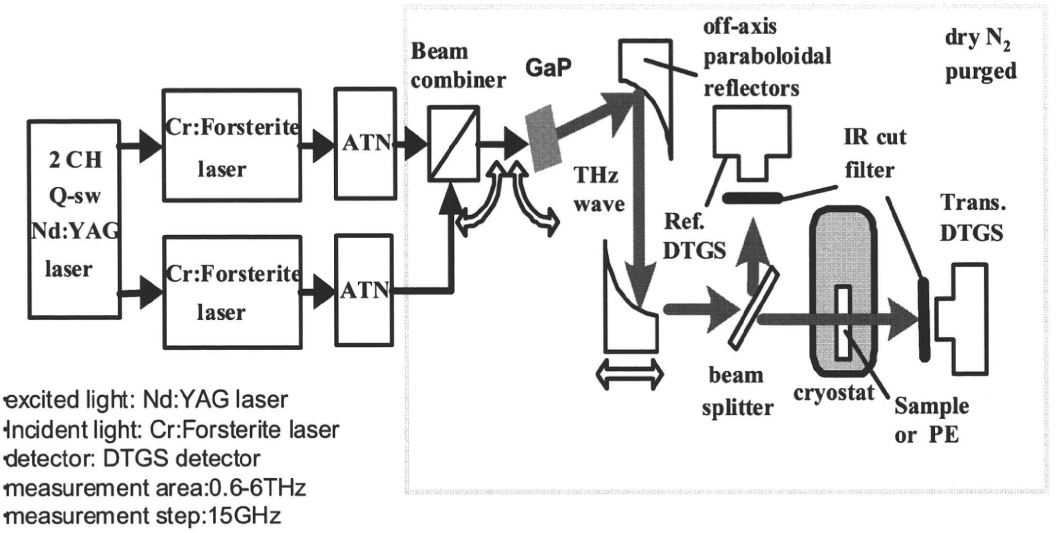

Figure 1: Schematic diagram of GaP-THz spectrometer via differential frequency generation

Results and Discussion

The baseline corrected THz spectra obtained from the purchased D-, L-, and leucine racemate are shown in Fig. 2(A). The peak at 3.7 THz was observed in both enantiomers. However, this single peak was shifted to 3.6 THz in racemate and the half width of the peak height of the enantiomers (0.7 THz) was narrowed to 0.4 THz. The baseline corrected THz spectra obtained from the re-crystallized mixtures are shown in Fig. 2(B). The intensity (a relative absorption coefficient) of D-leucine was approximately 20 % higher than that of DL-leucine. On the other hand, L-leucine showed 20 % lower intensity than that of racemate. No significant difference was observed about the waveforms, the peak position, and the half width of peak height at 3.7 THz between D- and L-leucine. In case of the mixtures, the peak positions were shifted to lower side of frequency, and the half width of peak height at 3.7 THz also became narrow as well as the purchased leucines. In order to investigate the THz peaks, the peak separation by Gaussian function was carried out. The single peak at 3.7 THz was separated to one main peak and 2 sub-peaks. Figure 3 shows the correlations between the spiked amount of L-form and the peak positions or the integrated values of peaks. Although the peak positions of the main peak were same in all mixtures, the peak positions of the sub-peaks of L- or D-form-rich mixture came up to that of the racemate. These results suggest that the existence of the other enantiomer would affect the phonon of crystallized leucine molecules. On the other hand, the correlation between the integrated values and the spiked amount of L-leucine shows the integrated values of the main peak were smallest on the D- or L-form-rich mixture resulting in a W-like pattern. The highest integrated value of the low sub-peak was observed in the D- or L-form-rich mixture, and shows an inverted W-like pattern. Moreover, the integrated value of L-leucine was comparatively higher than that of D-leucine. The peak integrated value of D-form-rich mixture of the high sub-peak was small, but it became bigger as the D-form content was increased. Furthermore, the integrated value in L-enantiomer remarkably increased and the value doubled compared with that of D-enantiomer. These results suggest that those values of D- or L-leucine were influenced by the existence of the other enantiomer, and the value of the high sub-peak at 4.1THz had correlated with the spiked content of D- or L-leucine in the re-crystallized mixture. The baseline corrected THz spectra obtained from the purchased D-, L-, and DL-alanine (Racemate) are shown in Fig. 4(A). Each optical isomer shows 2 peaks at 3.2 THz and 3.4 THz, racemate has the single peak at 3.1 THz. After re-crystallization, the two peaks on the THz waveform on D- or L-enantiomer were shifted to 4.2 THz and 4.4 THz. Moreover, the single peak of racemate was shifted to 4.1 THz on the THz wave obtained from L-form-rich or D-form-rich mixture (Fig. 4(B)). These results suggest that crystalline forms were changed from those of the purchased alanines because the distributor of these reagents would have done a different purification process from the re-crystallization method which was used in this study. In the THz waveform of the re-crystallized racemate, an increase of the relative molar absorbance was observed as the spiked content of D-enantiomer increased. In the THz waveform obtained from the purchased D- and L-alanine, small differences were observed at the frequency range from 2.1 THz to 2.8 THz.

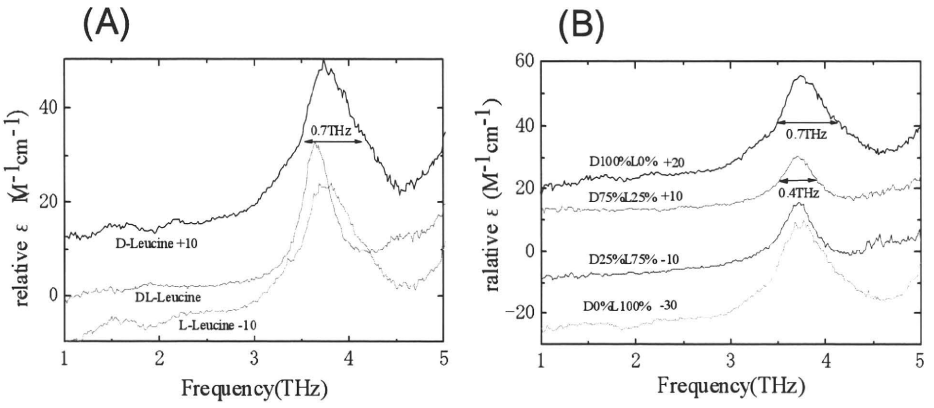

Figure 2: THz spectra of leucines (A: D-, L-, and DL-leucine (racemate) as purchased B: four kinds of re-crystallized D- and L-mixture)

In order to characterize the small differences, the curve separation was employed. Figure 5 shows the calculated D- and L-alanine waveforms by the Gaussian function. The three main peaks at 2.25 THz (No.1), 2.45 THz (No.2) and 2.6 THz (No.3) and the sub-peak at 2.7 THz (C) were calculated from the waveform of D-enantiomer. In case of L-enantiomer, the intensity of the peak No.2 became smaller compared with that of D-enantiomer. Moreover the two sub-peaks at 2.2 THz and 2.35 THz appeared and then the sub-peak C which was observed in D-enantiomer disappeared. While no significant differences between both enantiomers about the peak positions and the integrated values of peaks were observed, the peak intensities at the peak No.2 and No.3 of L-enantiomer were smaller than D-enantiomer. Although further study is necessary to explain the detail of these observations, the purchased D- and L-alanine may be distinguishable using THz spectroscopy.

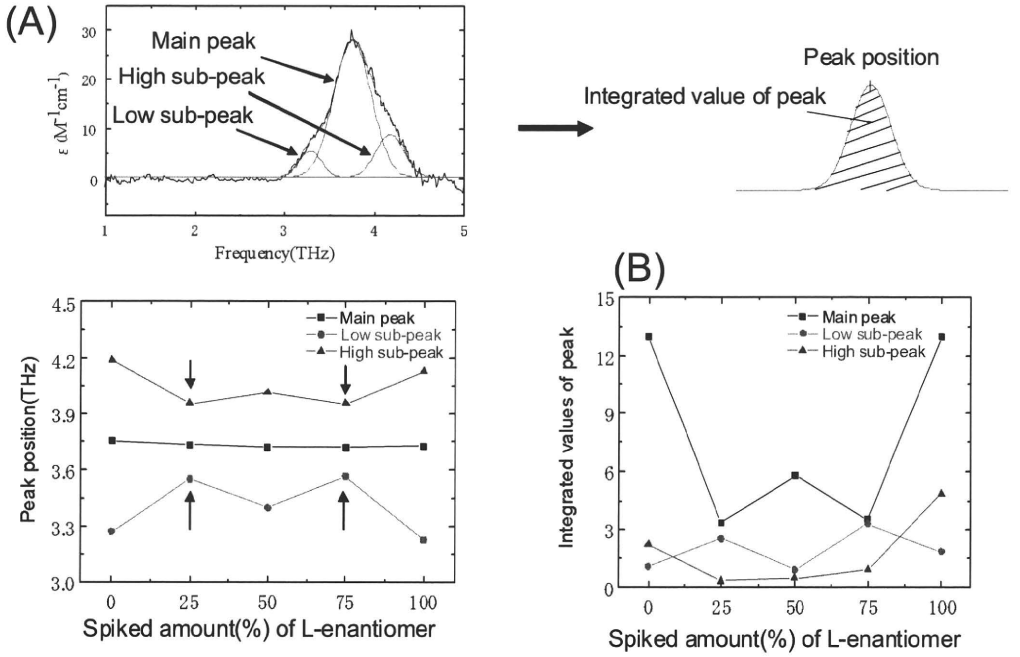

Figure 3: Correlations between re-crystallized mixtures and THz peaks (A: Peak positions (THz), B: Integrated values of peaks)

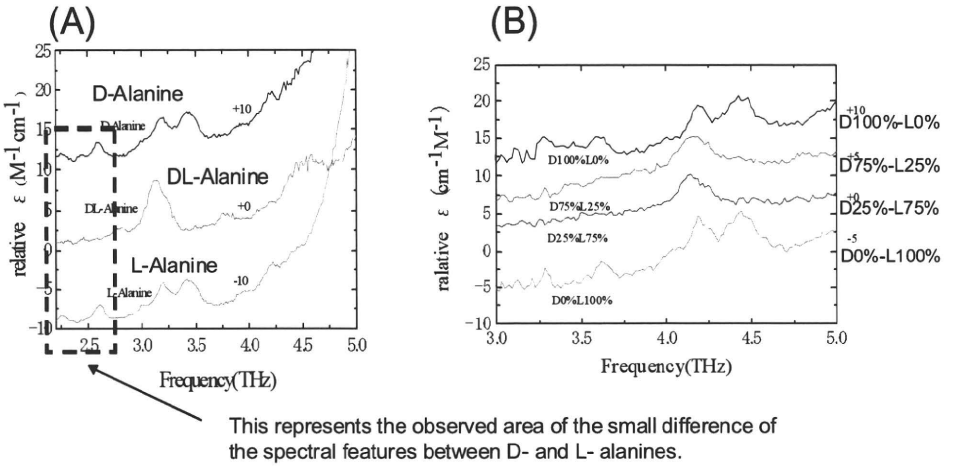

Figure 4: THz spectra of alanines (A: D-, L-, and DL-alanine (racemate) as purchased B: four kinds of re-crystallized D- and L-mixture)

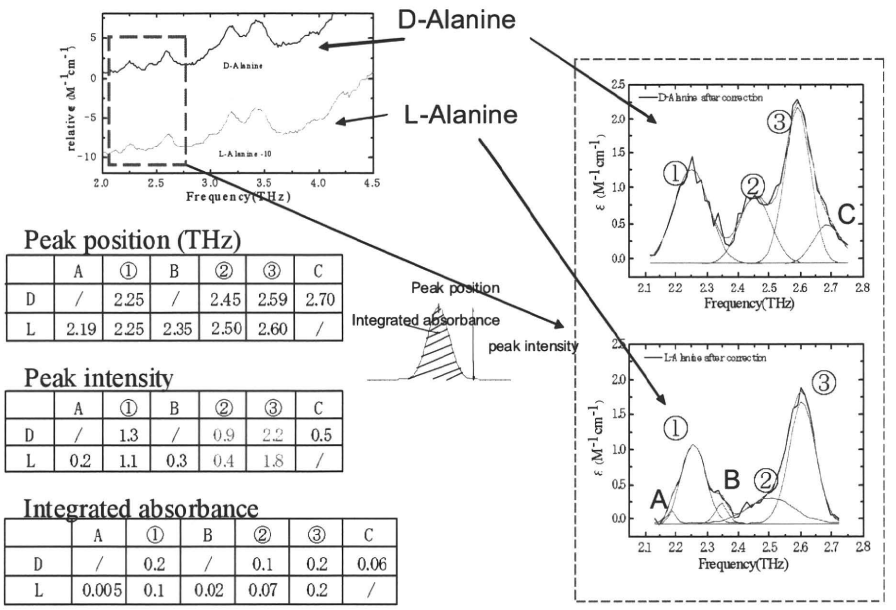

Peak position (THz)

	A	①	B	②	③	C
D	/	2.25	/	2.45	2.59	2.70
L	2.19	2.25	2.35	2.50	2.60	/

Peak intensity

	A	①	B	②	③	C
D	/	1.3	/	0.9	2.2	0.5
L	0.2	1.1	0.3	0.4	1.8	/

Integrated absorbance

	A	①	B	②	③	C
D	/	0.2	/	0.1	0.2	0.06
L	0.005	0.1	0.02	0.07	0.2	/

Figure 5: Fitted THz peaks of alanine and calculation results of three evaluation parameters

While comparative large two peaks (from 4.1 THz to 4.6 THz) were observed in D- or L-leucine, only single peak was detected in racemate and the re-crystallized mixtures. The authors are thinking that a hydrogen bond network of racemate which has a crystal structure formed by distributing of D- and L-enantiomer alternately is different from a hydrogen bond network in a crystal structure of each enantiomer. For example, a hydrogen network in three-dimensional structure of D- or L-enantiomer can be illustrated as Fig. 6 based on the crystalline structure of L-enantiomer (20).

On the other hand, a hydrogen bond network of racemate is formed by distributing both enantiomers alternately. Then a single molecule in crystal formed from D- or L-form molecule may construct a hydrogen bond network ([-O --- H-N-]) between adjacent two molecules. In case of racemate, D- or L-form molecule may construct two hydrogen networks between the other L- and D-form molecules (Fig. 7). The authors predict that inter-molecular vibration modes detected in THz spectra are correlated with an infra-red activity mode. Symmetry of crystal structure between enantiomer and racemate is different. Then, an infra-red active inter-molecular mode in enantiomer might change into an inactive mode in racemate. And

the opposite changing may be also observed. Of course further investigation is necessary to test this hypothesis; a difference of configuration to take high-density and/or stable crystal structure may affect THz spectral features.

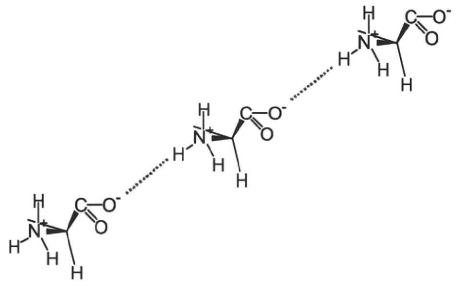

Figure 6: The image of a hydrogen bond between L-leucine and an adjacent one (Only one hydrogen bond is shown here.)

The different spectral feature between D- and L-alanine was observed in the range from 2.1 THz to 2.8 THz. In the calculated three peaks, the intensity of the peak No.2 was significantly decreased. Moreover, different calculated sub-peaks pattern between D- and L-enantiomer was observed as described in the paragraph 3.2. D- and L-enantiomer has the identical physical properties except an optical rotation. Although there is a possibility that an impurity derived from a different purification process between D- and L-leucine may cause spectral differences, it also has possibility that THz spectroscopy can sensitively detect small differences concerning a hydrogen bond network or a crystal lattice vibration.

A difference of spectral features between D- and L-leucine was not observed, but the differences of the integrated values of the peaks (shown in Fig. 5) obtained from the two sub-peaks between racemate and L- or D-form-rich mixture were observed. The optical rotation of re-crystallized mixture, L0%-D100%, L25%-D75%, L50%-D50%, L75%-D25% and L100%-D0% were -15.74 ± 0.02°, -0.06 ± 0.01°, 0.10 ± 0.02°, 0.12 ± 0.01° and 15.58 ± 0.01°, respectively. An isomerization in the aqueous solution and a thermo-isomerization of enantiomer was not observed. According to these results, According to these results, these re-crystallized mixtures did not include whole spiked amounts of L- or D-enantiomer. Most of these mixtures were formed by racemate, and a portion of excess L- or D-enantiomer was distributed in these crystals. Furthermore, no significant difference of the optical rotation between L50% and L75% mixtures was calculated. Thus, it is presumed that a racemization of D- and L-leucines in the solution was first progressed and then a portion of excess D- or L-enantiomer was taken in the racemate crystals. Although investigation of crystal structure of these mixtures is necessary to explain this observation, each D- or L-form-rich mixture showed the characteristic THz spectral features.

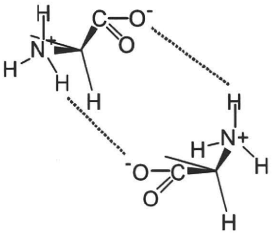

Figure 7: The image of assumed hydrogen bonds between two adjacent molecules in racemate

Conclusion

In this study, distinguishability of chiral compounds by THz spectroscopy was examined. Characteristic spectral differences between enantiomers and mixtures were observed by detailed analysis of spectral features. Because THz electro-magnetic wave can detect small but meaningful differences of crystal structure, more applications of THz electro-magnetic wave to analyze and to evaluate crystalline state and physical properties will be expected in the future.

Acknowledgement

This study was supported in part by a research grant from the Ministry of Health, Labour and Welfare of Japan (H20-iyaku-ippan-004).

References

1. P.F. Taday, I.V. Bradley, D.D. Arnone, M. Pepper, (2003) Using terahertz pulse spectroscopy to study the crystalline structure of a drug: a case study of the polymorphs of ranitidine hydrochloride, *J. Pharm.Sci.*, **92,** 831-838
2. M. Walther, B.M. Fischer, P.U. Jepsen (2003), Noncovalent intermolecular forces in polycrystalline and amorphous saccharides in the far infrared, *Chem. Phys.*, **288,** 261-268
3. C.J. Strachan, T. Rides, D.A. Newnham, K.C. Gordon, M. pepper, P.F. Taday, (2004) Using terahertz pulsed spectroscopy to study crystallinity of pharmaceutical materials, *Chem. Phys. Lett.*, **390,** 20-24
4. J.A. Zeitler, D.A. Newnham, P.F. Taday, T.L. Threlfall, R.W. Lancaster, R.W. Berg, C.J. Strachan, M. Pepper, K.C. Gordon, T. Rades, (2006) Characterization of temperature induced phase transitions in the five polymorphic forms of sulfathiazole by terahertz pulsed spectroscopy and differential scanning calorimetry, *J. Pharm. Sci.*, **95,** 2486-2498
5. J.A. Zeitler, D.A. Newnham, P.F. Taday, C.J. Strachan, M. Pepper, K.C. Gordon, T. Rades, (2005) Temperature dependent terahertz pulsed spectroscopy of carbamazepine, *Thermochimica Acta,* **436**, 70-76
6. C.J. Strachan, P.F. Taday, D.A. Newnham, K.C. Gordon, J.A. Zeitler, M. Pepper, T. Rades, (2005) Using terahertz pulsed spectroscopy to quantify pharmaceutical polymorphism and crystallinity, *J. Pharm. Sci.*, **94**, 837-846
7. G.M. Day, J.A. Zeitler, W. Jones, T. Rades, P.F. Taday, (2006) Understanding the influence of

polymorphism on phonon spectra: Lattice dynamics calculations and terahertz spectroscopy of carbamazepine, *J. Phys. Chem. B*, **110,** 447-456

8. J.A. Zeitler, P.F. Taday, M. Pepper, T. Rades, (2007) Relaxation and crystallization of amorphous carbamazepine studied by terahertz pulsed spectroscopy, *J. Pharm. Sci.,* **96**, 2703-2709
9. M. Yamaguchi, F. Miyamaru, K. Yamamoto, M. Tani and M. Hangyo, (2005) Terahertz absorption spectra of L-, D-, and DL-alanine and their application to determination of enantiometric composition, *Appl. Phys. Lett.,* **86**, 053903-1-3
10. R. Nishikiori, M. Yamaguchi, K. Takano, T. Enatzu, M. Tani, U. Chandimal de Silva, N. Kawashita, T. Takagi, S. Morimoto, M. Hangyo and M. Kawase, (2008) Application of Partial Least Square on quantitative analysis of L-, D, and DL-tartaric acid by terahertz absorption spectra, *Chem. Pharm. Bull*, **56**, 305-307
11. T. Tanabe, K. Suto, J. Nishizawa, T. Kimura, K. Saito, (2003) Frequency tunable high power terahertz wave generation from GaP, *J. Appl. Physics*, **93,** 4610-4615
12. T. Tanabe, K. Suto, J. Nishizawa, K. Saito, T. Kimura, (2003) Frequency-tunable terahertz wave generation via excitation of phonon-polaritons in Ga, *J. Physics D: Appl. Physics,* **36,** 953-957
13. T. Tanabe, K. Suto, J. Nishizawa, K. Saito, T. Kimura, (2003) Tunable terahertz wave generation in the 3- to 7-THz region from GaP, *Appl. Physics letters*, **83**, 237-239
14. T. Tanabe, Y. Kozawa, K. Suto, J. Nishizawa, Y. Oyama, (2005) Observing the stimulated Raman gain spectra of solutions using an infrared pump pulse with narrow linewidth and a low-noise cw probe laser, *Int. J. Infrared and Millimeter Waves,* **26,** 881-892
15. J. Nishizawa, T. Sasaki, K. Suto, T. Tanabe, K. Saito, T. Yamada, T. Kimura, (2005) THz transmittance measurements of nucleobases and related molecules in the 0.4 to 5.8THz region using a GaP THz wave generator, *Optics Comminications*, **246**, 229-239
16. J. Nishizawa, T. Sasaki, K. Suto, T. Yamada, T. Tanabe, T. Tanno, T. Sawai and Y. Miura, (2005) THz imaging of nucleobases and cancerous tissue using a GaP THz-wave generator, *Optics Comminications,* **244**, 469-274
17. J. Nishizawa, T. Sasaki, K. Suto, T. Tanabe, T. Yoshida, T. Kimura and K. Saito, (2006) Frequency-Tunable terahertz-wave generation from GaP using Cr:Forsterite lasers, *Int. J. Infrared and Millimeter Waves,* **27,** 779-789
18. T. Tanabe, J. Nishizawa, K. Suto, Y. Watanabe, T. Sasaki, Y. Oyama, (2007)Terahertz wave generation from GaP with continuous wave and pulse pumping in the 1-1.2μm region, *Materials Transactions,* **48**, 980-983
19. J. Nishizawa, T. Sasaki, K. Suto, M.Ito, T. Yoshida, T. Tanabe, (2008) High-resolution GaP terahertz spectrometer and its application to detect defects in γ-irradiated glucose crystal, *Int. J. Infrared and Millimeter Waves,* **29,** 291-297
20. A.R. Taulbee, J.A. Heuser, W.U. Spendel and G.E. Pacey, (2009) Qualitative analysis of collective mode frequency shifts in L-alanine using terahertz spectroscopy, *Anal. Chem.,* 2664-2667

Division of Drugs[1], National Institute of Health Sciences, Tokyo, Japan; TeraView Limited[2], St John's Innovation Park, Cambridge, United Kingdom; TDDS Research Laboratory[3], Hisamitsu Pharmaceutical Co. Inc., Tsukuba; Bruker Optics K.K[4], Tokyo, Japan

Detection of tulobuterol crystal in transdermal patches using Terahertz pulsed spectroscopy and imaging

T. Sakamoto[1], A. Portieri[2], P. F. Taday[2], Y. Takada[3], D. Sasakura[4], K. Aida[3], T. Matsubara[4], T. Miura[4], T. Terahara[3], D. D. Arnone[2], T. Kawanishi[1], Y. Hiyama[1]

Received January 19, 2009, accepted February 21, 2009

Dr. Tamoaki Sakamoto, Division of Drugs, National Institute of Health Sciences, 1-18-1, Kami-yoga, Setagaya-ku, Tokyo 158-8501, Japan
tsakamot@nihs.go.jp

Pharmazie 64: 361–365 (2009) *doi: 10.1691/ph.2009.9022*

Applicability of a Terahertz Pulsed Spectroscopy (TPS) and a Terahertz Pulsed Imaging (TPI) for detection of tulobuterol (TBR) crystals in transdermal patches was investigated. Because TBR has high permeability in dermis, crystalline TBR in patch matrices contributes to controlling the release rate of TBR from a matrix. Therefore, crystalline TBR is one of the important factors for quality control of TBR transdermal tapes. A model tape that includes 5 w/w%, 10 w/w%, 20 w/w% or 30 w/w% of TBR was measured by TPS/TPI. TBR crystals in the matrices were successfully detected by TPI. Identification of TBR in an image of a crystal-like mass was done by comparison between the spectra of tapes and a TBR standard substance. These results indicate that TPS and TPI are applicable to identifying crystalline lumps of an active drug in tapes for quality control.

1. Introduction

Terahertz (THz) time-domain spectroscopy gives an electric field record of time delay due to the presence of material in a beam path with a higher refractive index when compared to a reference. Fourier-transformed waveforms from an electric field show a characteristic relationship between frequency and absorbance. Fourier-transformed waveforms provide information about not only intra-molecular vibration and lattice vibration, but also intermolecular forces and hydrogen bonds.

In the pharmaceutical industry, applications of TPS and TPI for discrimination of polymorphs (Taday et al. 2003; Walther et al. 2003; Strachan et al. 2004, 2005; Zeitler et al. 2005, 2006, 2007, Day et al. 2006) and for detecting unique waveforms of APIs have been reported. Thus, these technologies are expected to be used for qualitative and/or quantitative analysis (Taday et al. 2003; Upadhya et al. 2003; Ueno et al. 2006; Zeitler et al. 2006). In particular, THz spectroscopy has been used for detecting foreign materials in samples and for measuring the thickness of coatings (Fitzgerald et al. 2005; Zeitler et al. 2006; Ho et al. 2007).

Tulobuterol ((*R,S*)-2-tert-butylamino-1-(2-chlorophenyl) ethanol, TBR) transdermal tapes are used to cure bronchial asthma as a bronchodilator (β_2-blocker). TBR is one of the suitable compounds for systemic transdermal formulation because it has very high permeability into the keratin layer. The release rate of TBR from the matrix is controlled by the formation of lumps of TBR crystals. For this reason, crystallization of TBR in a matrix is an important factor assuring the quality of this tape. However, verifying the crystallization of an active drug is difficult because TDDS tapes (or patches) generally have a sandwich-like structure with a matrix between a liner and a supporting board. Although release testing is often used to evaluate "releasability", which is one of the physico-chemical properties of an active drug in transdermal pharmaceuticals, releasability is not a suitable parameter for evaluating crystallization of an active drug. In order to compensate for this disadvantage, development of an alternative method by which to observe crystallization of an active drug in a matrix through a liner and/or a supporting board is needed. This manuscript describes the applicability of one of the innovative non-destructive analytical techniques, TPS and TPI, for quality evaluation of TDDS tapes.

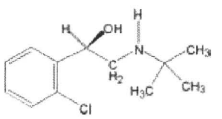

Tulobuterol

2. Investigations, results and discussions

2.1. THz pulsed spectrum of TBR obtained by TPS instrument

Fig. 1(A) shows the typical THz electric field records obtained from the TBR pellet and reference (PE pellet) by

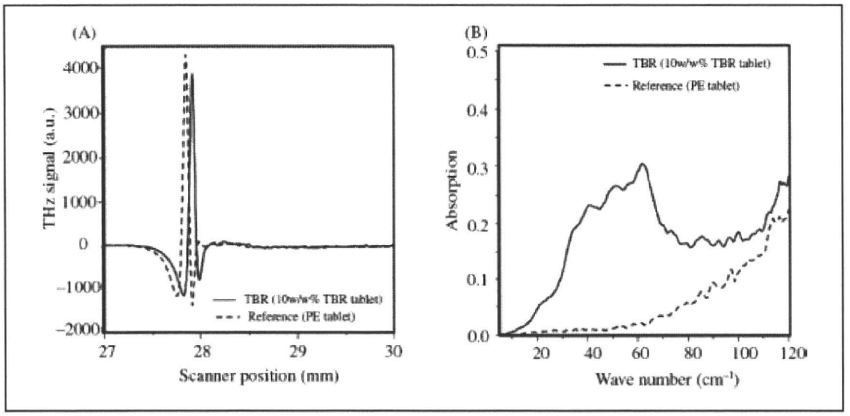

Fig. 1:
THz electric field records (A) and Fourier-transformed THz waveforms (B) of the TBR pellet and reference (PE pellet). The unique absorbance range, from 40 cm^{-1} to 70 cm^{-1}, is available to detect TBR absorbance

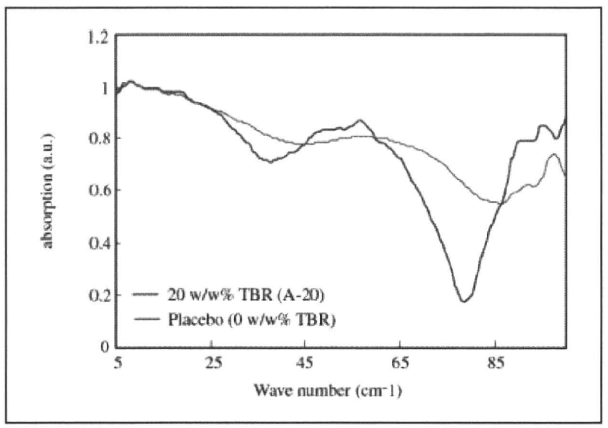

Fig. 2: THz spectra of model tape (20 w/w%, A-20) and placebo tape (0 w/w% TBR) obtained with quartz. The characteristic THz spectral range of TBR (from 45 cm^{-1} to 70 cm^{-1}) is best observed when etaloning effects are not dominating the range due to the thinness of the sample, as was the case here

the TPS 1000. The THz electric field record of the TBR pellet was shifted compared with that of the reference and the unique Fourier-transformed THz waveform of TBR was observed compared with that of the PE reference (Fig. 1(B)). This unique absorbance range, from 70 cm^{-1} to 45 cm^{-1}, seemed to be available to detect TBR absorbance from the total waveform of tapes.

2.2. THz image and spectra of TBR crystal in matrix

Fig. 2 shows the Fourier-transformed THz spectra of the placebo tape (the red line, an acrylic matrix) and the model tape (the blue line, 20w/w% TBR in an acrylic matrix, A-20). The fingerprint-like waveform of TBR from 70 cm^{-1} to 45 cm^{-1} was observed in the THz spectra obtained from the A-20. This observation suggests that chemical information of TBR can be detected in a tape. A lump of TBR crystals was detected at the top left of the image (Fig. 3(A)). The TPI contrast derives from refractive index differences. Therefore, it was presumed that the edge of the lumps of the TBR crystals contributed to making the definite contrast of shift of the refractive index. However, the image that is made from the shift of a refractive index would not provide chemical information about the lumps of TBR crystals. In order to identify the origin of the lumps of crystals, the THz spectra obtained from pixels which are located inside the lumps or outside the lumps were compared. Both spectra are shown in Fig. 3(B). The waveform indicated as the blue line represents the THz spectrum obtained from the pixel that is located inside the lump of crystals. The red line indicates the spectrum obtained from a pixel that is located outside the lump of crystals. The THz spectrum from the crystal shows a characteristic waveform range from 70 cm^{-1} to 45 cm^{-1}, almost the same as that of TBR standard substance. This observation strongly suggests that an image could be obtained from the crystal formed from TBR.

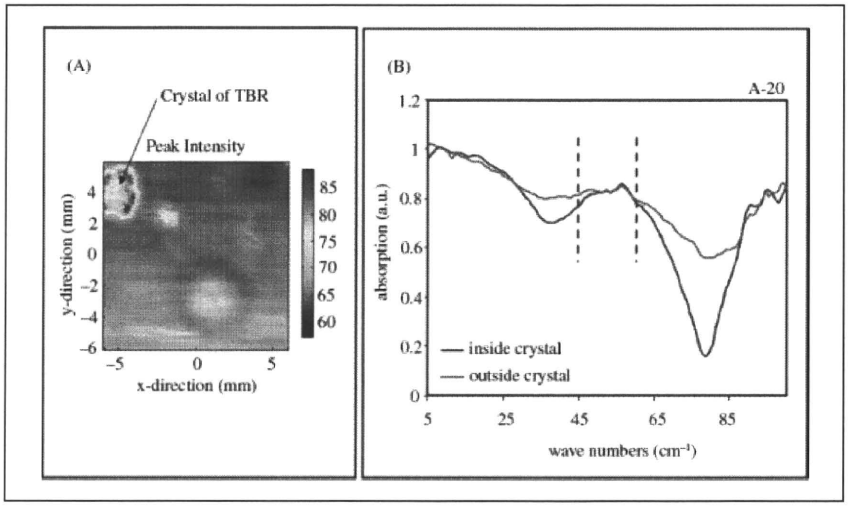

Fig. 3:
THz image of TBR crystal (A) and Fourier-transformed waveforms of pixels inside and outside of the crystals (B), obtained from A-20. The aggregation of TBR crystals which the arrow points to was clearly identified (A). It should be possible to observe the characteristic spectrum of TBR (from 45 cm^{-1} to 60 cm^{-1}) from both pixels located inside and outside of the crystal, but etaloning effects are again dominating the spectra

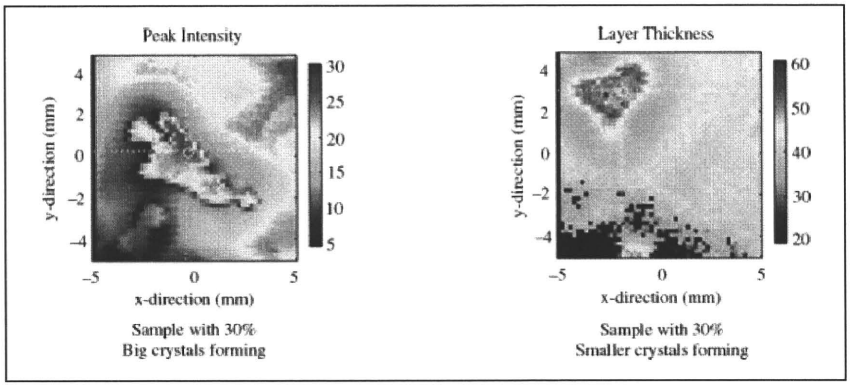

Fig. 4:
THz image of TBR crystals in matrix obtained using TPI 1000. Several sizes of TBR crystals were detected in the scanned area (the longer diameters: 0.5 mm to 3 mm, the shorter diameters: 0.1 mm to 0.2 mm)

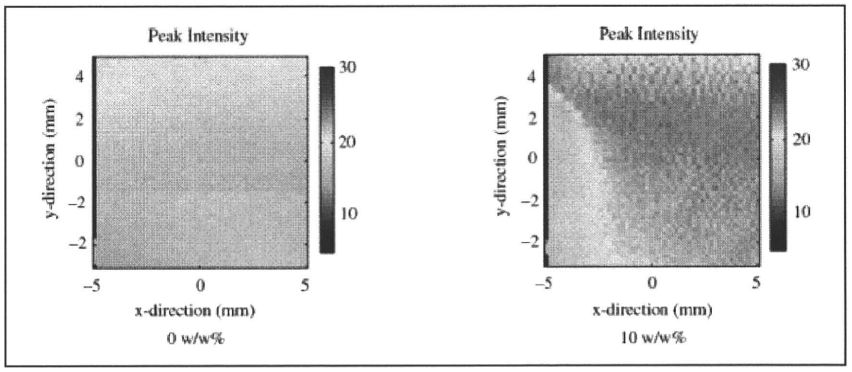

Fig. 5:
THz images of model tapes (0 and 10 w/w% TBR). Although there should be many small white crystals in R-10, only some were detected in the scanned area. In cases where the white crystals cannot be observed, the crystals might be smaller than the spatial resolution (100 μm) of TPI. Further studies need to be carried out to investigate differences in the samples

2.3. Size of crystals and spatial resolution of TPI

Fig. 4 shows the THz image obtained from the model tape (30 w/w% TBR, an acrylic matrix, A-30). Both model tapes were obtained from the same batch. Several sizes (short: 0.1 mm–0.2 mm, long: 0.5 mm–3 mm) of crystals were observed in these images.

The THz images obtained from the placebo tape (a rubber matrix, R-0) and the model tape (10 w/w% TBR, rubber matrix, R-10) are shown in Fig. 5. The image on the right side was obtained from R-10. Although small white crystals can be observed through a liner or a supporting board, no image of the lumps was observed in the THz image. This suggested that the sizes of the TBR crystals were smaller than the spatial resolution of TPI (approximately 100 μm). According to our study using Microscopic Laser Raman Spectroscopy/Mapping, the size of the TBR crystals was estimated to be from 6 μm to 40 μm (Sakamoto et al. 2006, 2007).

2.4. Depth image of crystals in TDDS tape

The THz image of A-30 and its depth image are shown in Fig. 6. The thickness of the lump of crystals in the matrix increased. The refractive index of the THz pulse was shifted due to the edges of the lumps of TBR crystals. This suggested that a comparatively big shift of a refractive index provides a definite image.

In conclusion, it was shown that THz spectroscopy/imaging technology was useful for detecting lumps of crystals of an active drug in transdermal tapes. THz spectroscopy/imaging can provide unique physical (and/or certain kinds of chemical) information compared with near infrared and/or mid infrared spectroscopy/imaging. In particular, obtaining a depth image from a pharmaceutical sample would be very useful for gaining an in-depth understanding of the quality of pharmaceuticals.

Although approximately 100 μm of spatial resolution in the THz pulsed image would hinder the detection of min-

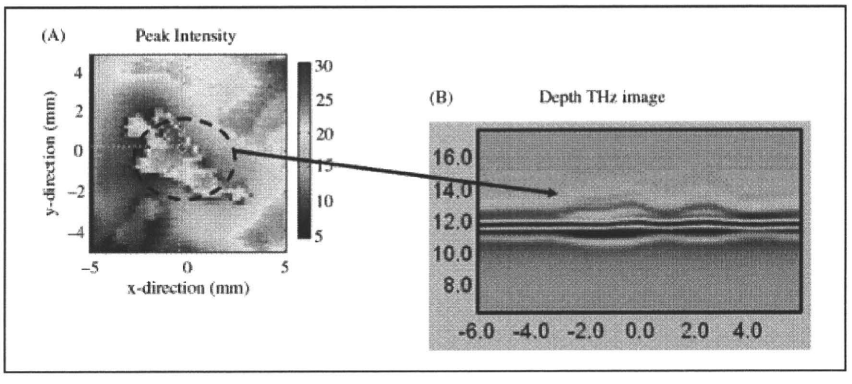

Fig. 6:
THz image of TBR crystal and depth THz image of matrix (A). The depth THz image in the scanned area where the crystal is observed shows the change in the thickness of the tape that can be seen (B)

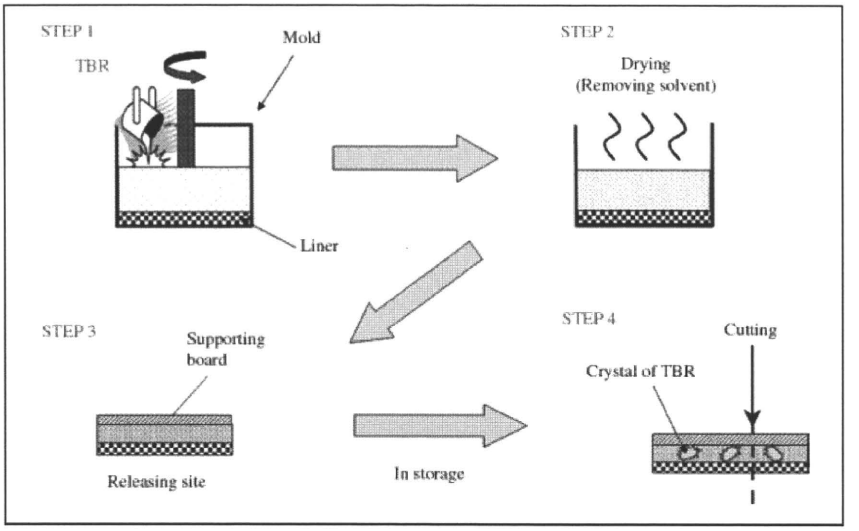

Fig. 7:
Flowchart showing preparation of model tapes. Residual solvents were removed by heating, and the mold was used to produce a sheet of model tape with a constant thickness and area

ute particles that are smaller than the spatial resolution, a reflective index of the THz pulsed wave may provide other useful information. Moreover, it would be able to detect problems caused by the manufacturing process, such as mixing of air bubbles and heterogeneity of active substances in the matrix. Therefore, this technology would be useful as an analytical tool not only for pharmaceutical quality control, but also for process control in pharmaceutical manufacturing.

Table: Prepared model transdermal tapes in this study

TBR level	Acrylic matrix	Rubber matrix
0 w/w% (Placebo)	A-0	R-0
10 w/w%	–	R-10
20 w/w%	A-20	–
30 w/w%	A-30	–

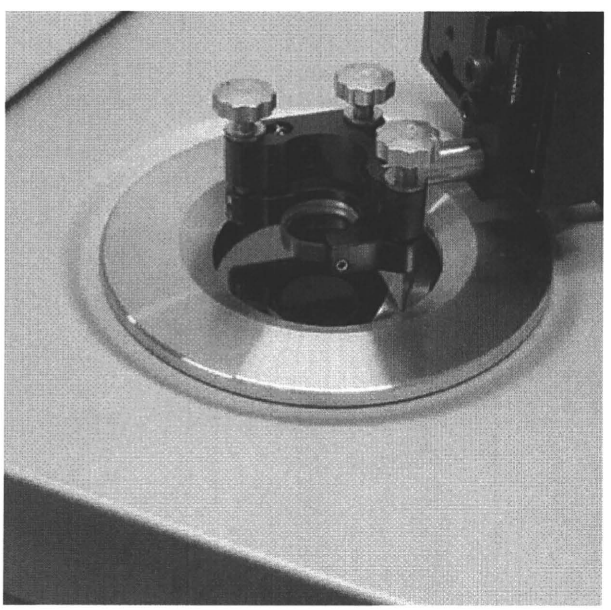

Fig. 8: Photograph of the metallic arm used when measuring the sample with a reference mirror

3. Experimental

3.1. Materials

TBR (purity > 99.0%) and model tapes were supplied by Hisamitsu Pharmaceutical Co Inc (Tokyo, Japan). Polyethylene (PE) powder of particle size < 80 μm was supplied by Induchem.

3.2. Model tapes

The model tapes were prepared by TDDS Laboratory, Hisamitsu Pharmaceutical Co Inc (Tsukuba, Japan). In order to identify crystals of TBR in the matrix, two kinds of matrices, rubber and acrylic matrices, were prepared. The flowchart for preparing the model tapes is shown in Fig. 7. TBR and other ingredients of the adhesive solutions were stirred in the mold adequately. The mixture was extended on the liner and residual solvents were removed by drying. When the thickness of the matrix (the adhesive layer) became a constant (approximately 50 μm thickness), a supporting board was pasted on the matrix after removing the mold. A polyethylene terephthalate (PET) film was selected as a liner and as a supporting board, for both the model and the placebo tape. And then these tapes cut to a size of 36 mm diameter. TBR crystals in model tapes were generated by leaving the tapes to crystallize for some time.
The model tape that contained 0 w/w% (R-0, placebo), 5 w/w% (R-5) or 10 w/w% (R-10) of TBR in a rubber matrix consisted of polyisobutylene, polybutene and lipocyclic petroleum resin. Small white crystals were seen in all areas of the matrix in the A-10 through a liner or a supporting board. The model tape that contained 0 w/w% (A-0, placebo), 20 w/w% (A-20) or 30 w/w% (A-30) of TBR in an acrylic matrix consisted of acryl adhesion polymer and isopropyl myristate. On the A-30 samples, small white crystals were seen in all areas of the matrices. A higher TBR concentration was needed to generate the crystals in the acrylic matrix compared with the rubber matrix because of the solubility of TBR. The prepared model tapes are shown in the Table.

3.3. Apparatus and measurements

3.3.1. Transmittance measurement of tablet by TPS

In order to identify a THz spectrum of TBR, a pellet containing approximately 10 w/w% of TBR was prepared by compressing at 2 t for 3 min with a press machine. The pellet was measured using a TPS 1000 spectrometer (TeraView Limited, Cambridge, UK). Each sample was measured covering the spectral range from 120 cm^{-1} to 2 cm^{-1} at 1.5 cm^{-1} of spectral resolution. Spectra were obtained averaging 1800 scans.

3.3.2. Transmittance-reflectance measurements of tapes by TPI

A reference mirror was first measured, and then the samples were mounted to the mirror and adjusted horizontally against the measurement window of the TPI Imaga^{TM} 1000 instrument (Fig. 8); subsequently, THz radiation was focused onto the samples to gain maximum sensitivity. Placebo tapes were used as a background for all measurements.
A TPI imaging system, TPI Imaga 1000 (TeraView Ltd., Cambridge, UK), was used for the reflectance measurement, which was operated in the rapid scan mode. Terahertz images were obtained by raster scanning the terahertz beam across the sample, which was mounted at the focus position. The scanned area was 12 mm × 12 mm, which corresponds to 120 pixels × 120 pixels at 100 μm spatial resolution. The total measurement time was approximately 30 min.

Acknowledgement: This study was supported in part by a research grant from the Ministry of Health, Labour and Welfare of Japan (H17-iyaku-ippan-040).

References

Day GM, Zeitler JA, Jones W, Rades T, Taday PF (2006) Understanding the influence of polymorphism on phonon spectra: Lattice dynamics calculations and terahertz spectroscopy of carbamazepine. J Phys Chem B 110: 447–456.

Fitzgerald AJ, Cole BE, Taday PF (2005) Nondestructive analysis of tablet coating thicknesses using terahertz pulsed imaging. J Pharm Sci 94: 177–183.

Ho L, Müller R, Römer M, Gordon KC, Heinämäki J, Kleinebudde P, Pepper M, Rades T, Shen YC, Strachan CJ, Taday PF, Zeitler JA (2007) Analysis of sustained-release tablet film coats using terahertz pulsed imaging. J Control Release 119: 253–261.

Sakamoto T, Fujimaki Y, Hiyama Y (2007) Study on development of quality analytical method using spectroscopic and imaging technique I. Application of Raman spectroscopy and mapping microscopy for quality evaluation of TDDS and Granules formulations. PharmTech Japan 23: 27–36 (in Japanese).

Sakamoto T, Matsubara T, Sasakura D, Takada Y, Fujimaki Y, Aida K, Miura T, Terahara T, Higo N, Kawanishi T, Hiyama Y (2009) Chemical mapping of tulobuterol in transdermal tapes using Microscopic Laser Raman Spectroscopy. Pharmazie 64: 166–171.

Strachan CJ, Taday PF, Newnham DA, Gordon KC, Zeitler JA, Pepper M, Rades T (2005) Using terahertz pulsed spectroscopy to quantify pharmaceutical polymorphism and crystallinity. J Pharm Sci 94: 837–846.

Strachan CJ, Rides T, Newnham DA, Gordon KC, Pepper M, Taday PF (2004) Using terahertz pulsed spectroscopy to study crystallinity of pharmaceutical materials. Chem Phys Lett 390: 20–24.

Taday PF, Bradley IV, Arnone DD, Pepper M (2003) Using terahertz pulse spectroscopy to study the crystalline structure of a drug: a case study of the polymorphs of ranitidine hydrochloride. J Pharm Sci 92: 831–838.

Ueno Y, Rungsawang R, Tomita I, Ajito K (2006) Quantitative measurements of amino acids by terahertz time-domain transmission spectroscopy. Anal Chem 78: 5424–5428.

Upadhya PC, Shen YC, Davies AG, Linfield EH (2003) Terahertz time-domain spectroscopy of glucose and uric acid. J Biol Phys 29: 117–121.

Walther M, Fischer BM, Jepsen PU (2003) Noncovalent intermolecular forces in polycrystalline and amorphous saccharides in the far infrared. Chem Phys 288: 261–268.

Zeitler JA, Newnham DA, Taday PF, Strachan CJ, Pepper M, Gordon KC, Rades T (2005) Temperature dependent terahertz pulsed spectroscopy of carbamazepine. Thermochim Acta 436: 70–76.

Zeitler JA, Shen YC, Baker C, Taday PF, Pepper M, Rades T (2006) Analysis of coating structure and interfaces in solid oral dosage forms by three dimensional terahertz pulsed imaging. J Pharm Sci 96: 330–340.

Zeitler JA, Newnham DA, Taday PF, Threlfall TL, Lancaster RW, Berg RW, Strachan CJ, Pepper M, Gordon KC, Rades T (2006) Characterization of temperature-induced phase transitions in the five polymorphic forms of sulfathiazole by terahertz pulsed spectroscopy and differential scanning calorimetry. J Pharm Sci 95: 2486–2498.

Zeitler JA, Taday PF, Pepper M, Rades T (2007) Relaxation and crystallization of amorphous carbamazepine studied by terahertz pulsed spectroscopy. J Pharm Sci 96: 2703–2709.

Division of Drugs[1], National Institute of Health Sciences; Bruker Optics K.K.[2], Tokyo; TDDS Laboratory[3], Hisamitsu Pharmaceutical Co Inc, Ibaraki; Tokyo Metropolitan Industrial Technology Research Institute[4], Tokyo, Japan

Chemical mapping of tulobuterol in transdermal tapes using Microscopic Laser Raman Spectroscopy

T. Sakamoto[1], T. Matsubara[2], D. Sasakura[2], Y. Takada[3], Y. Fujimaki[4], K. Aida[3], T. Miura[2], T. Terahara[3], N. Higo[3], T. Kawanishi[1], Y. Hiyama[1]

Received July 29, 2008, accepted August 5, 2008

Tomoaki Sakamoto, Ph.D., National Institute of Health Sciences, 1-18-1, Kami-yoga, Setagaya-ku, Tokyo 158-8501, Japan
tsakamot@nihs.go.jp

Pharmazie 64: 166–171 (2009) *doi: 10.1691/ph.2008.8217*

Microscopic Laser Raman Spectroscopy and Mapping (MLRSM) technique was used to investigate the distribution of tulobuterol (TBR) crystals in transdermal tapes. TBR is one of suitable compounds for the transdermal pharmaceuticals because it has high permeability into skin. In case of TBR transdermal tapes, some commercial products also contain TBR crystals in order to control a release rate from a matrix. Therefore, the presence of TBR crystals in the matrix is a critical factor for quality assurance of this type of TDDS tapes. The model tapes prepared here employed two kinds of matrices, i.e., rubber or acrylic, which are generally used for transdermal pharmaceuticals. TBR crystals in the matrix were observed by MLRSM. Accurate observation of the distribution of TBR in the tapes was achieved by creating a Raman chemical map based on detecting unique TBR peak in each pixel. Moreover, differences in the growth of TBR crystals in the two kinds of matrices were detected by microscopic observation. MLRSM also enabled the detection of TBR crystals in commercial products. The present findings suggest that Raman micro-spectroscopic analysis would be very useful for verifying and/or assessing the quality of transdermal pharmaceuticals in development, as well as for manufacturing process control.

1. Introduction

Tulobuterol (TBR) transdermal tapes are applied in cases of bronchial asthma as a bronchodilator (β_2-blocker). TBR suitable for use in transdermal drug delivery because it has high permeability into the keratin layer (Uematsu et al. 1993). TBR pharmaceutical products with a Transdermal Drug Delivery System (TDDS) have advantages such as eliminating the side effects including abdominal pain and appetite loss (Iikura et al. 1995), and maintaining effective blood TBR levels for approximately 24 h (Horiguchi et al. 2004). The release rate of TBR from the matrix is controlled by the formation of TBR crystals. The crystallization of TBR has the possibility of influencing the TBR blood level profile. Therefore, it is necessary to characterize not only the release rate of TBR from a matrix, but also to characterize its crystallinity in dosage form in the matrix. *In vitro* penetration testing using stripped animal skin and *in vitro* release testing have been used to evaluate transdermal pharmaceuticals in terms of penetration and release. Because these evaluation methods show only one of several alternative physicochemical parameters (e.g., release rate, rate of penetration rate of an active substance, etc.), it has remained difficult to clarify the chemical status and quality of transdermal pharmaceuticals. In case of transdermal tapes containing an active drug as crystals in a matrix, the active drug is slowly released from the matrix into the keratin layer, as crystals will gradually dissolve in a matrix. Therefore, the crystallization of TBR is an important quality parameter. However, evaluation of the correlation of release rates between animal skin and human skin using *in vitro* penetration testing of animal skin has also remained difficult. Therefore, it has become desirable to develop analytical methods of both microscopically and chemically detecting and observing crystals of active drugs in a matrix.

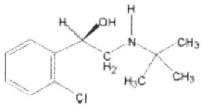

Tulobuterol (TBR)

Laser Raman spectroscopy is a method of spectroscopic analysis of spectra of Raman scattered light obtained by exposure of a sample to a laser. Raman spectroscopy has been used for the identification and quantification of polymorphs (Deely et al. 1991; Falcon et al. 2004; Ferrari et al. 2004; Findlay et al. 1998; Hu et al. 2005; Langkilde et al. 1997; Ono et al. 2004; Schöll et al. 2006; Starbuck et al. 2002; Wang et al. 2000; Murphy et al. 2005) and for monitoring the crystallization process (Taylor et al. 1998;

Murphy et al. 2005; Nørgaard et al. 2005) because it enables the detection of crystals, and in particular, differences between crystal forms. Therefore, Microscopic Laser Raman Spectroscopy/Mapping (MLRSM) was employed in the present study to microscopically and chemically detect TBR crystals in transdermal tapes. The applicability of this spectroscopic analytical method was examined both for the purpose of quality control (i.e., to confirm the crystals of TBR in the matrix), as well as with the aim of enhancing our understanding of relevant quality attributes of prototype pharmaceuticals in various stages of development.

2. Investigations and results

2.1. Determination of a unique wave number range in the Raman spectrum for TBR in model tapes

A typical Raman spectrum obtained from the TBR reference standard substance is shown in Fig. 1. Typical spectra of placebo tape (a) and model tape (b) of rubber matrices are shown in Figs. 2 and 3, respectively. To find characteristic wave numbers of TBR, these spectra were compared with the Raman spectrum obtained from a model tape. The peak bending vibration of C–C at 415cm^{-1} was used as the characteristic peak of TBR, and the integrated values obtained from the wave number range from 420 cm^{-1} to 400 cm^{-1} were used for making the Raman chemical maps.

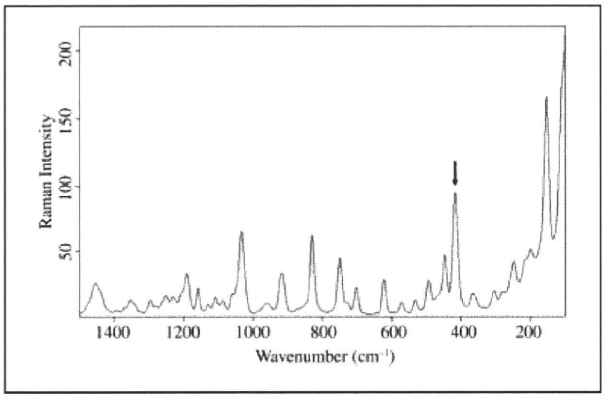

Fig. 1: Typical Raman spectrum of the TBR reference standard. The peak at 415 cm^{-1} was chosen as characteristic, because no interfering peak was observed in the vicinity of this peak

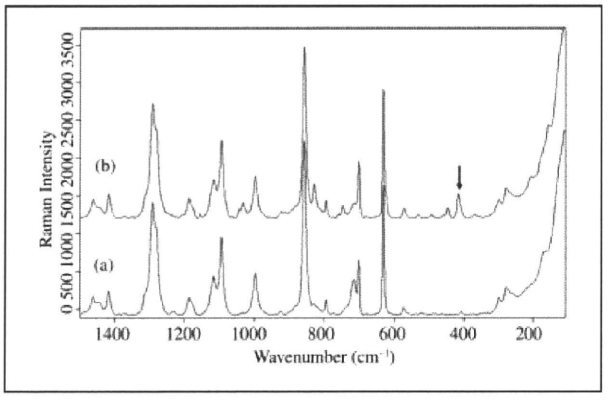

Fig. 2: Typical Raman spectra of placebo (a, rubber matrix) and model tape (b, rubber matrix). The arrow indicates the peak chosen for the specific detection of TBR. Comparatively strong intensity was observed

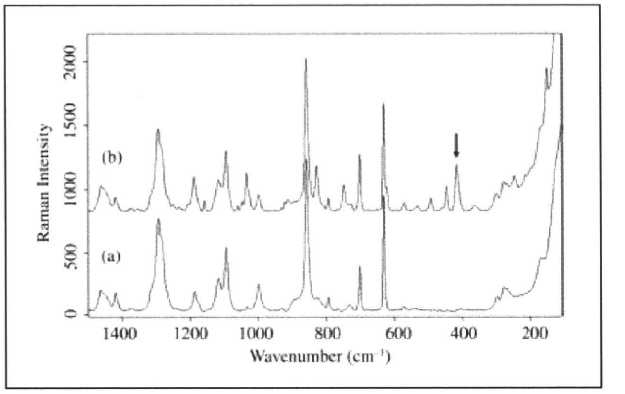

Fig. 3: Typical Raman spectra of placebo (a, acrylic matrix) and model tape (b, acrylic matrix). The very similar Raman spectrum of placebo tape was observed compared with that of the rubber matrix, because the absorption of supporting boards that were made from PET was also detected

2.2. Optical micrograph and Raman chemical mapping of the crystals of TBR in a rubber matrix

Figure 4a shows the micrograph of a 600 × 500 μm area in the R-10 sample. An enlarged micrograph (200 × 200 μm) is shown in Fig. 4b. Pillar-shaped crystals (short, 1 μm–2 μm; long, 10 μm–20 μm) that formed in lumps were observed. Figure 4c and d show the three-dimensional (3D) map and the Raman chemical map that corresponds with the area in Fig. 4b. In the Raman chemical map, the distribution of TBR in the matrix corresponded with the distribution of crystals in the optical micrograph. The Raman absorbance intensity corresponded with the distribution of optically observed TBR.

2.3. Optical micrograph and Raman chemical mapping of the crystals of TBR in an acrylic matrix

A micrograph of a 600 × 500 μm area and an enlarged micrograph of a 200 × 200 μm area of the A-20 sample are shown in Fig. 5a and b, respectively. In Figure 5c and d, the respective 3D chemical map and Raman chemical map are given that correspond to Fig. 5b. A lump of crystals with radiating branches was observed in the matrix. The Raman chemical map of TBR corresponding to the micrograph was obtained. The Raman chemical maps, which show the distribution of Raman chemical intensity, indicated trace amounts of crystal growth.

2.4. Shapes of crystals of TBR in two types of matrix

The micrograph of early-stage TBR crystallization in an acrylic matrix is shown in Fig. 6a. A lump of crystals with radiating branches was observed. Figure 6b shows the micrograph obtained approximately at the level of the top of branch of the crystal. The findings suggest that the pillar-shaped crystals were successively generated at the top of branches, and that the branches grew radially from the core. In case of the rubber matrix, pillar-shaped crystals that formed individual lumps were observed, as shown in Fig. 4a and b. No signs of a core were observed, and lumps of pillar-shaped crystals occurred individually in the matrix. These findings suggest that the TBR crystal growth mechanism differs in the two types of matrix analyzed here. Empirical evidence suggests that when crystallization was rapid, numerous crystalline lumps lacking a nucleus appeared in all areas of the ma-

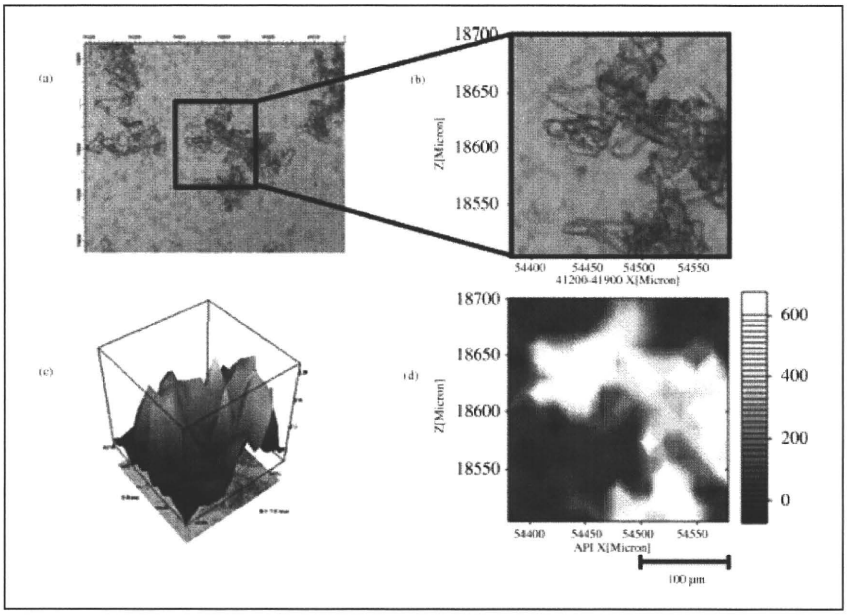

Fig. 4:
Micrographs and Raman chemical maps obtained from the model tape (R-10). a: Micrograph of a 600 × 500 µm area, b: Enlarged micrograph of a 200 × 200 µm area, c: 3D Raman chemical map that corresponds with that in d, d: Raman chemical map that corresponds with b. The distribution of the TBR crystals in the matrix was clearly detected by both methods

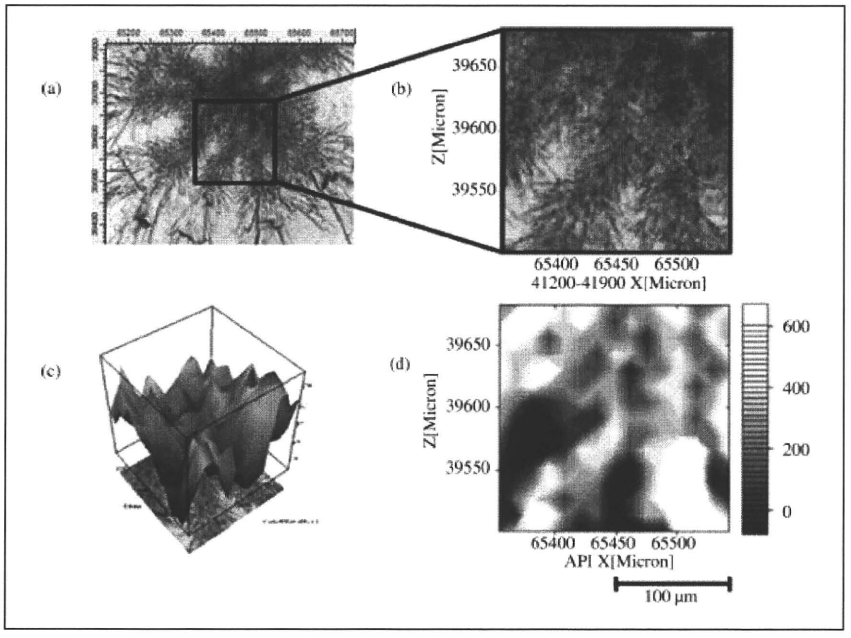

Fig. 5:
Micrographs and Raman chemical maps obtained from the model tape (A-20). a: Micrograph of a 600 × 500 µm area, b: Enlarged micrograph of a 200 × 200 µm area, c: 3D Raman chemical map that corresponds with d, d: Raman chemical map that corresponds with b. The mass of the crystals, with radiating branches, was observed in the matrix. The Raman chemical map of TBR corresponding to the micrograph was obtained

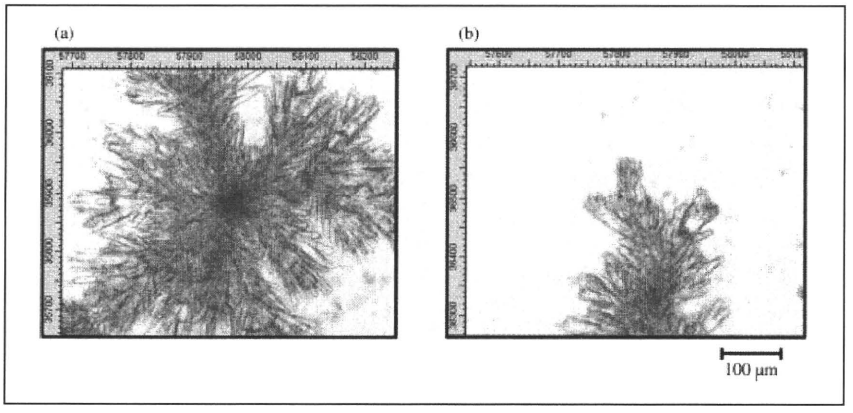

Fig. 6:
Micrographs of the mass of TBR crystals obtained from A-20. a: Core with radiating branches, b: Top of the branch. Pillar-shaped crystals generated successively at the top of branches were observed microscopically

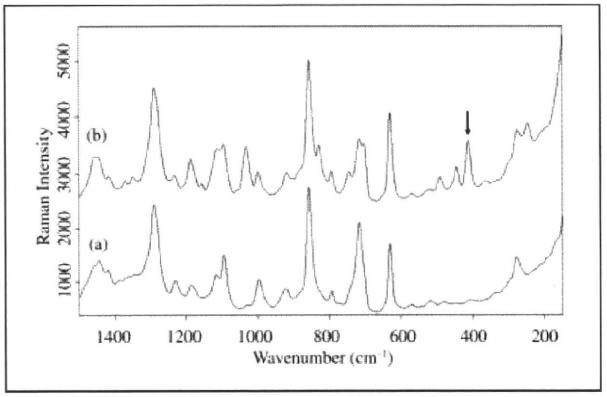

Fig. 7: Raman spectra of commercial tape. a: Background, b: The area where crystals were observed. The characteristic peak (415 cm^{-1}) of TBR was detected

trix, but in cases of slow crystallization, crystals formed around a nucleus. An empirical understanding of such processes would also suggest that the TBR crystals formed more rapidly in the rubber matrix than in the acrylic matrix. The processes of crystallization in these matrices agreed with the empirical evidence obtained here. It appears that new crystals will form around a nucleus, because surrounding molecules are stimulated to crystallize by a nucleus, as shown in Fig. 6. Raghavan et al. (2001) reported that the nucleation process depends in such cases on the hydrogen-bonding functional groups of not only the active drug, but also the polymer. Therefore, it appears likely that differences between the polymer structures of matrices contribute to differences in the process of crystal formation in those matrices. Although further study will still be needed to explain this phenomenon, it appears that the growth mechanism of TBR crystals in each matrix

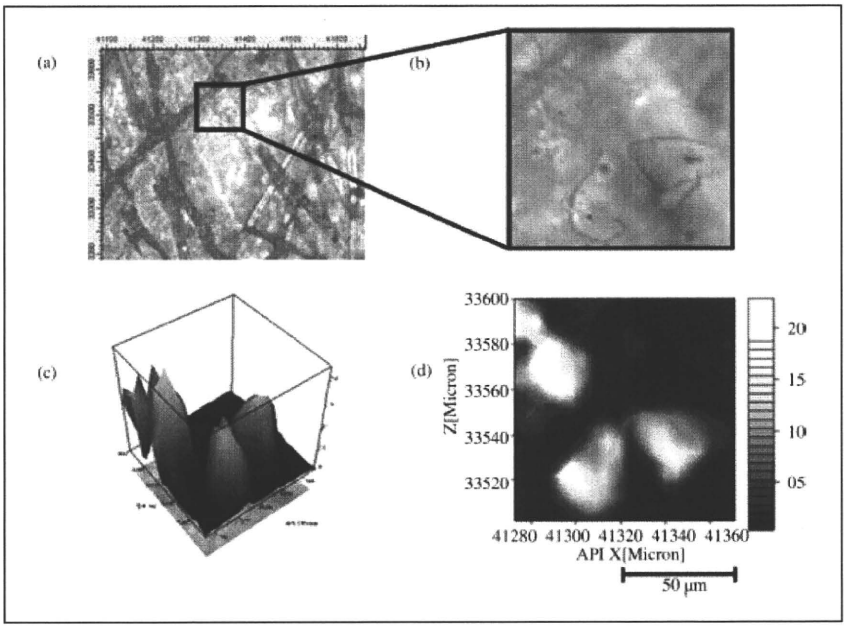

Fig. 8:
Micrographs and Raman chemical maps obtained from the commercial tape (1 mg TBR in the tape). a: Micrograph of a 570 × 450 μm area, b: Enlarged micrograph of a 100 × 100 μm area, c: 3D Raman chemical map that corresponds with d, d: Raman chemical map that corresponds with b. TBR crystals were clearly detected in the matrix

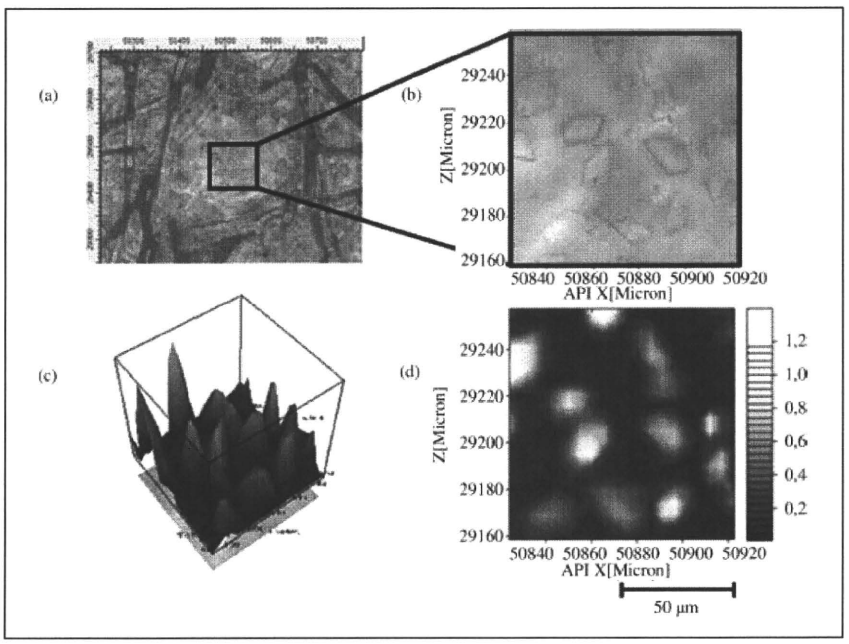

Fig. 9:
Micrographs and Raman chemical maps obtained from commercial tape (2 mg TBR in tape). a: Micrograph of a 570 × 450 μm area, b: Enlarged micrograph of a 100 × 100 μm area, c: 3D Raman chemical map that corresponds with d, d: Raman chemical map that corresponds with b. The crystal distribution suggested that rubber matrix was used for these products

may depend in part on hydrogen bonding between functional groups of TBR and the polymer.

2.5. *Analysis of commercial products using MLRSM*

MLRSM was used here to detect TBR crystals in commercial products. In these samples, there was a supporting board made of cloth, and a liner made of a white, plastic-like material. The tapes were measured after the liner was removed. Figure 7 shows the Raman spectra of commercial tape. Figure 7a or b were obtained from the area where crystals were not observed or the area where crystals were observed, respectively. The characteristic peak of TBR at 415 cm^{-1} was detected. Figures 8 and 9 show the micrographs (a and b) and the Raman chemical maps (c and d) obtained from the commercial product, Hokunalin® tape, examined in 1 mg and 2 mg sizes, respectively. Areas in which TBR crystals were observed were selected for obtaining the Raman chemical maps. In both micrographs, more crystals appeared to be present in the 2 mg tape than in the 1 mg tape. However, according to the documentation for this product, several sizes of tape, prepared by cutting sections from a larger sheet, can yield various products. Therefore, the TBR content in a particular unit area in several types of Hokunalin® tapes will remain equivalent. It has been hypothesized that the number of crystals in a measured area is affected by the area selected for mapping. Moreover, TBR crystals were also observed that did not assume the lump-shaped formation in this product. Round, pillar-shaped crystals ranging in size from 6×15 μm to 30×40 μm were also observed. The formation of TBR crystals in the product was similar to that observed in a model tape made of a rubber matrix. Helpful information was provided in the attached documentation regarding the medical additives (e.g., polyisobutylene, polybutene, and lipocyclic petroleum resin) used to prepare the rubber matrix. The results of the present study suggest that the crystal formation patterns in a matrix yield useful information about unique matrix characteristics.

3. Discussion

The application of MLRSM to detect the crystals of an active drug in transdermal tapes has been studied. In the case of these TDDS pharmaceutical products, microscopy and chemical mapping method were useful for evaluating the quality of these products as non-destructive spectroscopic technology. Moreover, MLRSM could be used to measure products equipped with a liner for the purpose of quality control during processing, as well as to assess the crystallization of an active drug during storage. Non-destructive spectroscopic methods may be used for analysis of the chemical state and distribution of an active drug, not only in the case of transdermal tapes, but also in film-form products in pharmaceutical development. Furthermore, these methods could be applied as analytical tools to evaluate various factors affecting product quality in the manufacturing process.

4. Experimental

4.1. *Microscopic Laser Raman Spectroscopy and Mapping (MLRSM) instrument and measurement conditions*

MLRSM measurement was performed using the SENTERRA Dispersive Raman Microscope (Bruker Optics K.K., Germany). Excitation wavelength, laser power, integration time, number of scans, spatial resolution and grating were set at 785 nm, 100 mW, 10 s, 1 scan, 2 μm and 1200 lines/mm, respectively.

4.2. *Materials*

Tulobuterol (TBR, purity > 99.0%) was provided by Hisamitsu Pharmaceutical Co., Inc. (Tokyo, Japan). 2-Ethylhexyl acrylate vinylpyrrolidone copolymer, isopropyl myristate, polyisobutylene, polybutene, and lipocyclic petroleum resin for matrices of model patches were used as Japanese Pharmaceutical Excipients (JPE)-quality products. Hokunalin® Tape (1 mg and 2 mg) (Maruho Co. Ltd., Osaka, Japan) were purchased from a commercial source.

4.3. *Preparation of model tapes*

Model tapes were prepared by the TDDS Laboratory, Hisamitsu Pharmaceutical Co., Inc. (Tsukuba, Japan). In order to identify crystalline lumps of TBR in the matrix, two types of matrix, rubber and acrylic, were prepared. TBR and other matrix adhesive solution ingredients were mixed and thoroughly stirred. The mixture was extended on a liner and residual solvents were removed by drying. The matrix was adjusted to a constant thickness (approximately 50 μm) and pasted onto a supporting board. A polyethylene terephthalate (PET) film was selected for the liner and the supporting board of the model tapes. Then, the sample was cut to a size of 36 mm diameter. TBR crystals in the model tapes were generated by leaving the sample to stand for one week (a rubber matrix) or one month (an acrylic matrix).

Model tapes were prepared that contained 0w/w% (R-0, placebo), and 10 w/w% (R-10) of TBR in a rubber matrix that consisted of polyisobutylene, polybutene, and lipocyclic petroleum resin. Small white crystals were seen in all areas of the matrix in the R-10 sample. Model tapes were prepared that contained 0 w/w% (A-0, placebo) and 20 w/w% (A-20) of TBR in an acrylic matrix composed of acrylic adhesive polymer and isopropyl myristate. Due to the solubility of TBR, higher TBR concentrations were necessary to generate crystals in the acrylic matrix than in the rubber matrix.

4.4. *Measurement of model tapes and commercial products*

The model tapes with the liner were placed on a measurement stand with the liner side facing up. For the measurement of the model tapes, micrographs were obtained and chemical mapping was performed by microscopically focusing on crystals of interest. For the MLRSM measurements of the commercial TBR transdermal tapes, the tapes were placed without the liner on the measurement stand, with the adhesive side facing up.

Acknowledgement: This study was supported in part by a research grant from the Ministry of Health, Labour and Welfare (H17-iyaku-ippan-040).

References

Deely C, Spragg R, Threlfall T (1991) A Comparison of Fourier transform infrared and near-infrared Fourier transform Raman spectroscopy for quantitative measurements: an application in polymorphism. Spectrochim Acta 47: 1217–1223.

Falcon J, Berglund K (2004) In situ monitoring of antisolvent addition crystallization with principal components analysis of Raman spectra. Cryst Growth Des 4: 457–463.

Ferrari E, Davey R (2004) Solution-mediated transformation of α to β l-glutamic acid: rate enhancement due to secondary nucleation. Cryst Growth Des 4: 1061–1068.

Findlay P, Bugay D (1998) Utilization of Fourier transform-Raman spectroscopy for the study of pharmaceutical crystal forms. J Pharm Biomed Anal 16: 921–930.

Horiguchi T, Kondo R, Miyazaki J, Torigoe H, Tachikawa S (2004) Clinical evaluation of tulobuterol patch in patients with mild or moderate persistent bronchial asthma-effects of long-term treatment on airway inflammation and hypersensitivity. Nihon Kokyuki Gakkai Zasshi 42: 132–137.

Hu Y, Liang J, Myerson A, Taylor LS (2005) Crystallization monitoring by Raman spectroscopy: simultaneous measurement of desupersaturation profile and polymorphic form in flufenamic acid systems. Ind Eng Chem Res 44: 1233–1240.

Iikura Y, Uchiyama H, Akimoto K, Ebisawa M, Sakaguchi N, Tsubaki T, Ishizu H, Kabayama H, Yagi K, Miura K (1995) Pharmacokinetics and pharmacodynamics of the tulobuterol patch, HN-078, in childhood asthma. Ann Allergy Asthma Immunol 74: 147–151.

Langkilde F, Sjöblom J, Tekenbergs-Hjelte L, Mrak A (1997) Quantitative FT-Raman analysis of two crystal forms of a pharmaceutical compound. J Pharm Biomed Anal 15: 687–696.

Murphy BM, Prescott SW, Larson I (2005) Measurement of lactose crystallinity using Raman spectroscopy. J Pharm Biomed Anal 38: 186–190.

Nørgaard L, Hahn MT, Knudsen LB, Farhat IA, Engelsen SB (2005) Multivariate near infrared and Rama spectroscopic quantifications of the crystallinity of lactose in whet permeate powder. Int Dairy J 15: 1261–1270.

Ono T, ter Horst J, Jansens P (2004) Quantitative measurement of the polymorphic transformation of l-glutamic acid using in-situ Raman spectroscopy. Cryst Growth Des 4: 465–469.

Raghavan SL, Trividic A, Davis AF, Hadgraft J (2001) Crystallization of hydrocortisone acetate: influence of polymers. Int J Pharm 212: 213–221.

Schöll J, Bonalumi D, Vicum L, Mazzotti M (2006) In situ monitoring and modeling of the solvent-mediated polymorphic transformation of l-glutamic acid. Cryst Growth Des, 6: 881–891.

Starbuck C, Spartails A, Wai L, Wang J, Fernandez P, Lindemann C, Zhou G, Ge Z (2002) Process optimization of a complex pharmaceutical polymorphic system via in situ Raman spectroscopy. Cryst Growth Des 2: 515–522.

Taylor LS, Zografi G (1998) Quantitative analysis of crystallinity using FT-Raman spectroscopy. Pharm Res 15: 755–761.

Uematsu T, Nakano M, Kosuge K, Kanamaru M, Nakashima M (1993) The pharmacokinetics of the beta 2-adrenocepter agonist, tulobuterol given transdermally and by inhalation. Eur J Clin Pharmacol 44: 361–364.

Wang F, Wachter J, Antosz F, Berglund K (2000) An investigation of solvent-mediated polymorphic transformation of progesterone using in situ Raman spectroscopy. Org Proc Res Dev, 4: 391–395.